CERN/SPSC 2000-037/P319
CERN, 14/09/2000

$\bar{p}$-nucleus Interactions at Low Energies with a Streamer Chamber at AD

The STRAD Collaboration

A. Bianconi[a], G. Bonomi[a], M.P. Bussa[a], M. Corradini[a], A. Donzella[a], E. Lodi Rizzini[a,*], L. Venturelli[a], R. Vilar[a], A. Zenoni[a], E.M. Andreev[b], N.S. Angelov[b], T.D. Blokhinstseva[b], V.A. Butenko[b], V.A. Drozdov[b], V.N. Frolov[b], V.M. Grebenyuk[b], V.V. Ivanov[b], V.I. Lyashenko[b], A.S. Moiseenko[b], V.A. Panyushkin[b], V.I.Pryanichnikov[b], N.A. Russakovich[b], O. Y. Shevchenko[b], W. Joffrain[c], V. Lagomarsino[c], G. Manuzio[c], F. Balestra[d], L. Busso[d], L. Fava[d], L. Ferrero[d], G. Piragino[d], G.B. Pontecorvo[d], F. Tosello[d], G. Zosi[d]

a) Dipartimento di Chimica e Fisica per l'Ingegneria e per i Materiali, Università di Brescia, Brescia and INFN Sez. di Pavia, Pavia, Italy
b) Joint Institute for Nuclear Research, Dubna, Moscow, Russia
c) Dipartimento di Fisica Università di Genova and INFN Sez. di Genova, Genova, Italy
d) Dipartimento di Fisica Generale "A. Avogadro", Università di Torino and INFN Sez. di Torino, Torino, Italy

*Spokeperson, *e-mail address:* lodi@fidabs.ing.unibs.it

1 Introduction

The dynamics of the antiproton-nucleus interaction and the structure of the nucleus appear to affect in an unexpected way the behavior of the $\bar{p}A$ annihilation cross section at low energies. In light nuclei the $\bar{p}d$ and $\bar{p}^4He$ annihilation cross sections at $\bar{p}$ momentum below 60 MeV/c drop to the $\bar{p}p$ level, whereas at higher momenta ($\gtrsim$ 100 MeV/c) the $\bar{p}$ nucleus annihilation cross section increases regularly with the number of nucleons in the nuclei[1].
The recent low statistics measurement of the $\bar{p}^{20}Ne$ annihilation cross section at 57 MeV/c seems to confirm a saturation effect of σ_{ann} with the mass number A at decreasing $\bar{p}$ momentum (see fig.1), in agreement with the description of strong interaction effects in hadronic atoms, including $\bar{p}$ atoms.

Moreover, a low statistics measurement in ^3He obtained a value similar to the ^{20}Ne one, thus supporting a strong dependence on the nucleus structure. This result confirms the importance of the separation energy of protons observed by the PS209 experiment on level width and shift of the antiprotonic atoms.
To understand the behavior of $\sigma_{ann}(\bar{p}A)$, experiments are needed to confirm first the existing low statistics measurements, and new measurements should be performed on $\bar{p}$ annihilation with heavier nuclei and at even lower energies. The detector proposed is a Self-shunted Streamer Chamber operated at atmospheric pressure or lower. The peculiar feature of this visualizing technique is that the filling gas acts both as detecting medium and as nuclear target. The detector can be also equipped with internal solid targets and in the proposed set-up the filling gas is a proper admixture of noble gases with different atomic weights.
The apparatus is able to detect and measure both fast light particles and slow fragments produced in $\bar{p}A$ annihilation. Therefore, a good separation among annihilations on protons, α particles and medium-heavy nuclei is possible. A good spatial resolution on the $\bar{p}$ incoming track and on the vertex is also obtainable. Thus, the apparatus is able to identify annihilations affected by a previous elastic scattering.
Moreover, $\bar{p}p$ elastic scattering measurements may clarify the resonant behavior recently suggested in $\bar{p}p$ interactions at $\bar{p}$ momenta below 200 MeV/c.
Since the $\bar{p}$ will slow down and eventually stop in the gas admixture inside the Streamer Chamber, the pictures collected will contain both annihilations in flight and at rest. As a consequence, from these pictures it will be possible to extract the first direct information on the relative probability of $\bar{p}$ atomic capture on binary systems of noble gases. In this field our proposed measurements will be complementary to the ASACUSA $\bar{p}A^+$ capture measurements.

1.1 The $\bar{N}$-nucleus , $\bar{N}$-nucleon interaction at low energies

The measurements performed at LEAR in '80 on $\bar{p}$ [2] and $\bar{n}$ [3] annihilation on nuclei at momenta ranging from 600 down to 200 MeV/c show a behaviour $\sigma_{ann} = \sigma_o A^\nu$ with $\nu \approx 2/3$ (see fig. 2,3 and fig. 4,5) . The behaviour of σ_R with the incident momentum is similar for all nuclei and follows that of the $\bar{p}p$ interaction. This suggests a picture where the dominant reaction mechanism is the $\bar{N}N$ annihilation on quasi-free nucleons and the differences in σ_R among the nuclei are explainable in terms of eclipse effects, which reduce the probability that a target nucleon is "seen" by the incident antinucleon.
At 200 MeV/c this picture of the $\bar{p}$-nucleus annihilation is questionable but experimental data on $\bar{p}$ ^{20}Ne and $\bar{p}$ ^4He are still in agreement with the $A^{2/3}$ law. Antineutron data [4] also follow this behavior from 280 MeV/c down to $\approx$ 60 MeV/c on target nuclei from intermediate to heavy.
On the contrary antiproton annihilation on light nuclei at momenta below 100 MeV/c seems to be very weakly dependent on the mass of the target nucleus against any naive expectation of a scaling law with the number of nucleons in

the target. A set of recent measurements of antiproton-nucleus annihilations [5, 6, 7, 8] and of widths and shifts of antiprotonic atoms [9, 10, 11], together with several model analyses [12, 13, 14, 15, 16, 17, 18, 19, 20, 21, 22, 23, 24] have demonstrated that huge saturation effects dominate the $\bar{p}$-nucleus interaction, both in the negative energy bound state domain and in the positive energy reaction sector.

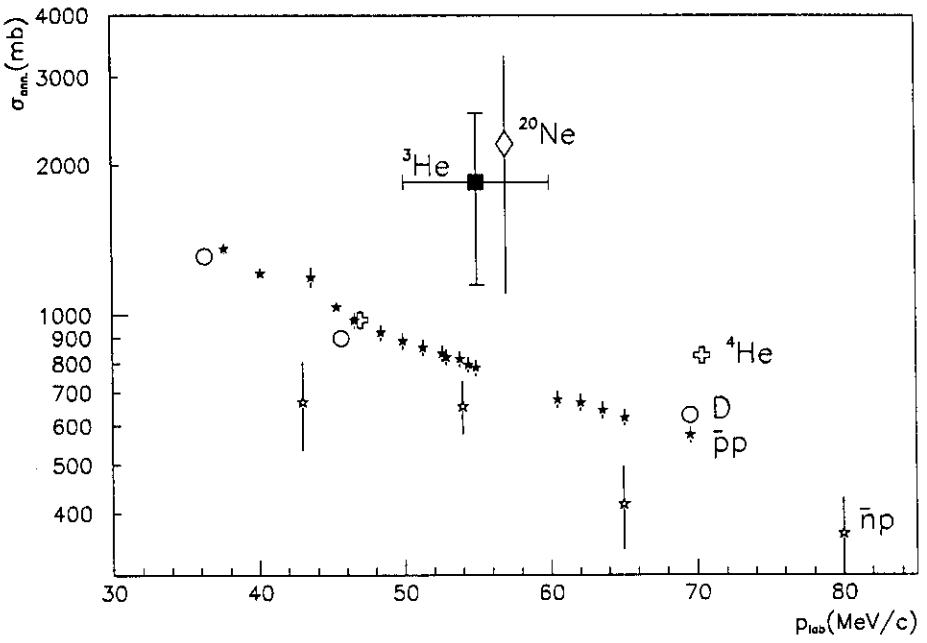

Figure 1: Antiproton annihilation cross sections for D, ^3He, ^4He and Ne. Full stars and empty stars correspond respectively to $\bar{p}p$ and $\bar{n}p$ data. See text for references.

An "intersection" point at laboratory momentum 30 - 60 MeV/c exists (fig.1) such that $\bar{p}$-deuteron and $\bar{p}-^4$He annihilation cross sections are larger than $\bar{p}p$ annihilation cross sections at larger momenta, but smaller at smaller momenta. Data on these nuclei are satisfactorily precise, but they are not enough to interpolate univocally the energy dependence of their annihilation rate below 100 MeV/c with S-wave even more dominant. Moreover, low-statistics data on $\bar{p}^{20}Ne$ and $\bar{p}^3He$ annihilation at about 60 MeV/c [7, 8] exist. When Coulomb

effects are subtracted, the Neon result has the same size as that of $\bar{p}p$, while the ^{3}He result is twice as large as the others (including ^{4}He) at the same momentum. Below 200 MeV/c no elastic data are available on light nuclei, nor antiproton data of any kind on medium and heavy nuclei. The $\bar{n}A$ annihilation does not show any violation of the $A^{2/3}$ law down to 60 MeV/c, but the available data refer to nuclei with $A > 12$.
The difference between antineutron data on heavy nuclei and antiproton data on light nuclei can be explained in terms of the number of partial waves involved in the two cases, and also by the lower momentum at which the antiproton data have been taken.

On the interpretation side, it has been recently observed [20, 21, 22] that for low energy annihilations on nuclei a strong suppression has to be expected on the very general ground that large annihilation rates would contradict the Heisenberg uncertainty principle. It was demonstrated that annihilation cross sections should be approximately independent on the target mass number A, apart for Coulomb and surface effects. This result is in agreement with the optical potential calculations [14, 18, 24] at least at very small momenta. These studies suggest that bulk nuclear matter effects are not relevant in the $\bar{p}$-nucleus physics at small energy, and Coulomb effects can be understood and subtracted [20]. Indeed, most of the above quoted potential models, and also phenomenological analyses [25, 26, 27] for the annihilation process suggest that the $\bar{N}N$ and $\bar{N}$-nucleus annihilation processes take place in a thin spherical shell placed just outside the nuclear surface. This mechanism prevents any investigation of the target structure at low energies, but makes the annihilation an ideal tool for probing the details of the external region of the nucleus, such as the neutron/proton ratio at the nuclear surface or the extraction energy of the peripheral nucleons. Following the suggestions of the experiments on antiprotonic atoms, a certain correlation should exist between the annihilation probability and the extraction energy of the most peripheral nucleon, even if this correlation is not always verified and data on isotopes look contradictory [28]. Among the positive energy data available, ^{3}He and ^{4}He data seem to confirm the relevance of the extraction energy of the most peripheral nucleon, while deuteron data contradict it. Indeed, according to this point of view, deuteron annihilation rates should be larger than ^{3}He ones (Coulomb effects apart), which should be larger than ^{4}He ones. Seemingly, the N/Z composition at the nuclear surface has a non negligible role [23], in agreement with the fact that $\bar{n}p$ annihilation rates are lower than $\bar{p}p$ ones at momenta 50-200 MeV/c [29]. It has also been remarked [28, 30] that some nuclear anomalies can be explained in terms of the presence of a sub-threshold resonance (predicted by potential models, see e.g.[31, 32, 33, 34, 35, 36, 37, 38]) that, while not evident in over-threshold $\bar{p}p$ data, would heavily affect nucleon-antinucleon interactions in close $\bar{N} - N$ configurations in nuclei (characterized by large negative two-body center of mass energies). It must be stressed that in the momentum range $70 - 115\ MeV/c$ measurements of $\bar{p}p$ annihilation cross section are lacking and $\bar{p}p$ elastic scat-

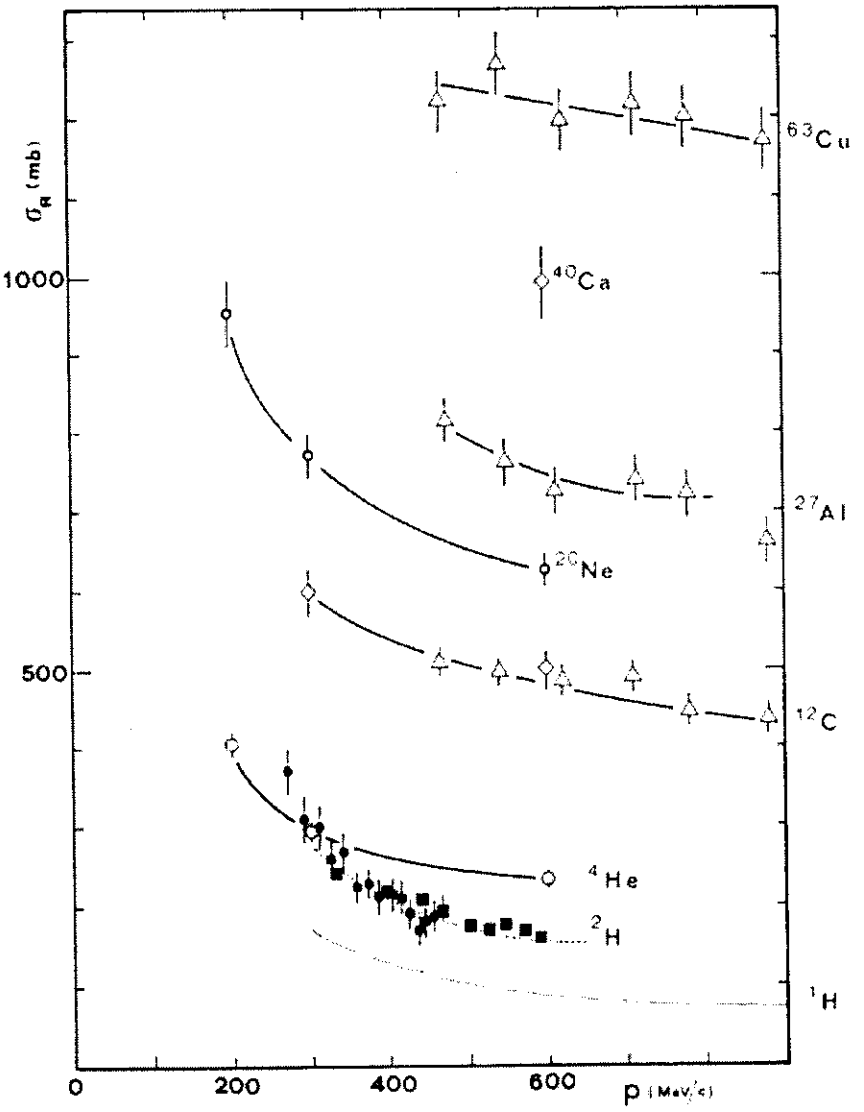

Figure 2: Comparison among reaction cross sections at different $\bar{p}$ momenta ($p_{\bar{p}} \geq 200 MeV/c$).

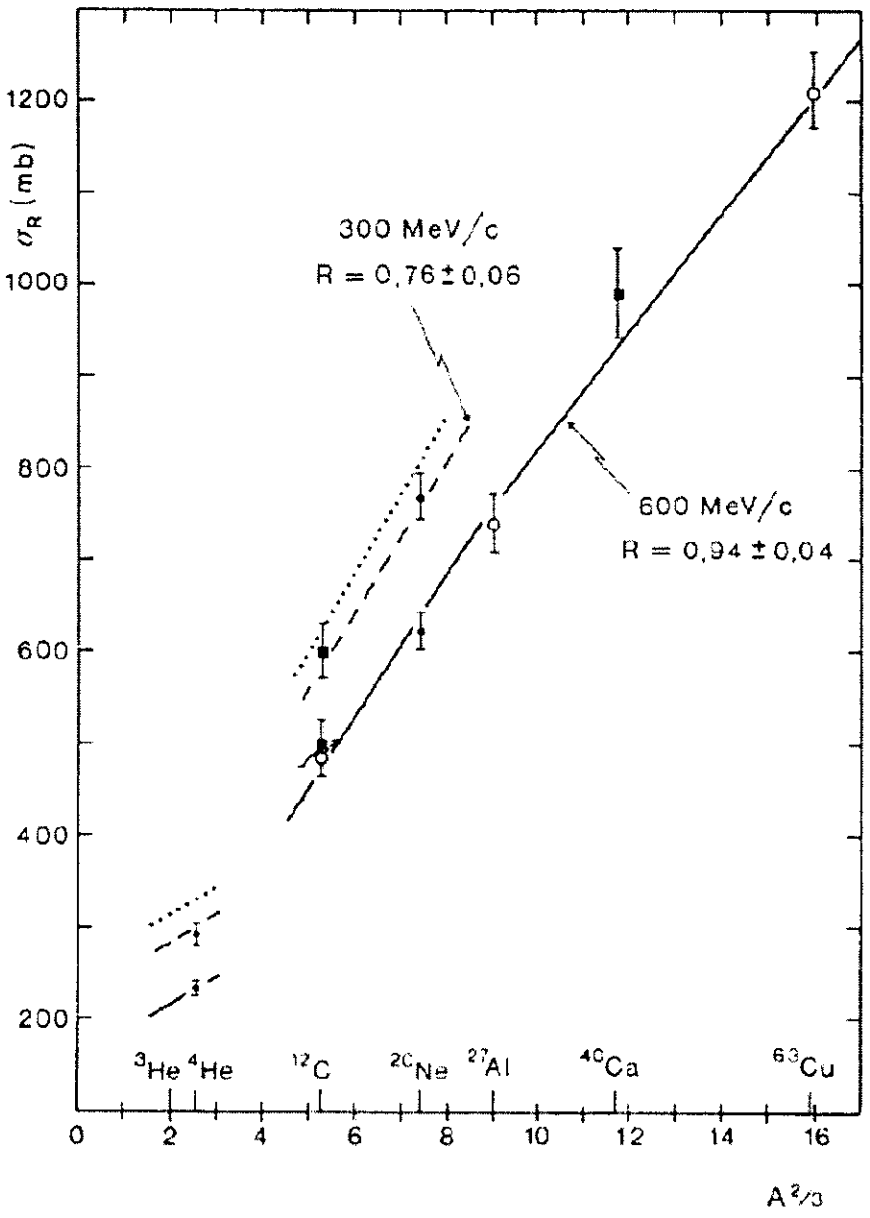

Figure 3: $\bar{p}A$ reaction cross section data versus $A^{2/3}$ at 300 and 600 MeV/c. Full and dashed lines are the result of fits with Glauber Theory.

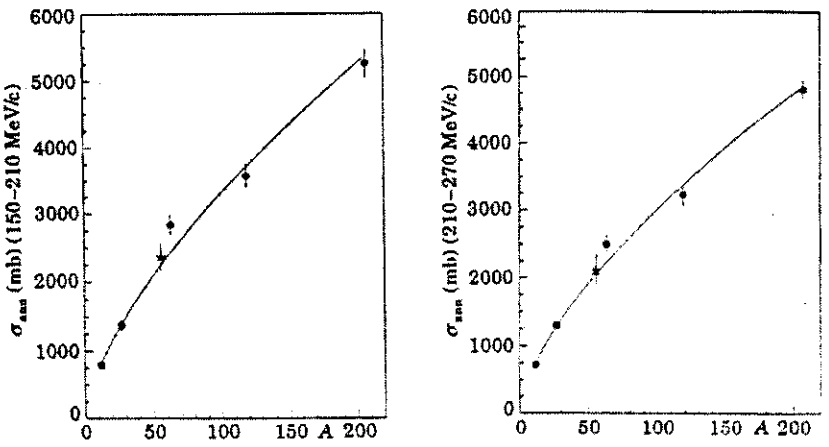

Figure 4: $\bar{n}A$ annihilation cross section for $\bar{n}$ momentum in the intervals (150-210) MeV/c and (210-270) MeV/c. The curves correspond to a fit to A^{ν} with $\nu \approx 2/3$.

tering data start at 200 MeV/c. New data on both $\bar{p}p$ annihilation and elastic scattering below $100 MeV/c$ could help in disentangling this problem.
A clear interpretation of these points is prevented in the case of antiprotonic atoms by the difficulty in accessing to the lowest partial waves. In the scattering/annihilation case the real obstacles are the scarcity and lack of systematicity of the available data. In presence of more complete sets of data, well-tested few-body techniques exist that would permit to relate data on light nuclei with subnuclear interactions (at least in the case of deuteron, ^{3}He and ^{4}He). On the other side, a comparison between data on light and heavy nuclei could permit to understand the real role of general quantum principles and of the nuclear surface.

1.2 the $\bar{p}A$ capture

Atomic capture of heavy negative particles has been studied almost since the discovery of these particles. The theory was pioneered by Fermi and Teller [39, 40] using the Thomas-Fermi model for the target atom.
The negative particle feels an increasingly attractive potential as it approaches the nucleus. One or more electrons can be ionized as the negative particle is captured. In this process multiple electronic continua come into play and electron-electron as well as exotic particle-electron correlations may be important.
Moreover, it could be inferred from some experimental observations of relative

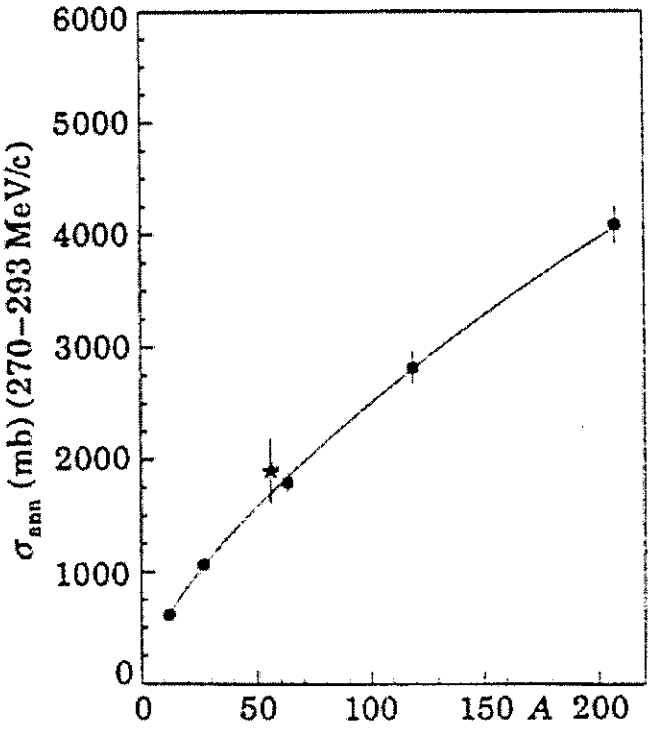

Figure 5: $\bar{n}A$ annihilation cross section for $\bar{n}$ momentum in the interval (270-293) MeV/c.

capture probabilities that additional electrons tend to increase the capture probability, though not monotonically; simple Z scaling [39] is clearly inadequate. The opposite supposition, that the capture cross section depends mainly on the target ionization potential, as suggested by capture occurring mainly at low collision energies, is also clearly inconsistent with the data. Cohen [41] developed calculations on helium and neon, the simplest atoms for which experiments have been performed. The results are shown in Table 1.
Following Cohen, the most informative way of looking at capture is the reduced capture ratio, i.e. the ratio of capture probabilities *per atom*

$$A(Z_1, Z_2) = \frac{W(Z_1)/c(Z_1)}{W(Z_2)/c(Z_2)} \tag{1}$$

where $W(Z_i)$ is the probability of capture by the component i in a binary mixture and $c(Z_i)$ is the atomic concentration of each species. If the process

is linear in Z then this ratio is independent of $c(Z_i)$; however this ratio in fact depends more or less significantly on the concentration. The reduced capture ratios for $\bar{p}$ and μ^- in Ne:He mixtures are shown in fig. 6 and fig. 7 respectively.

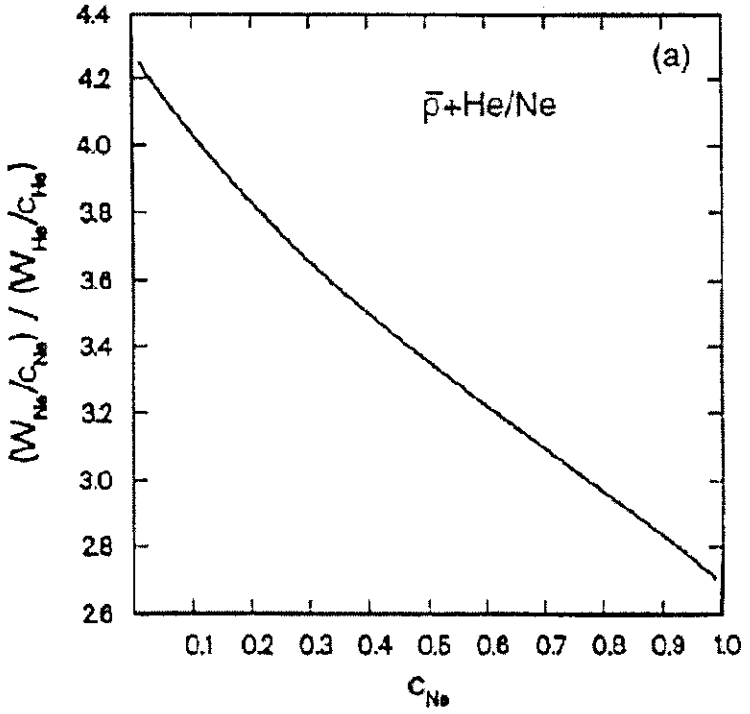

Figure 6: Reduced capture ratio for $\bar{p}$ in He/Ne.

In both cases the probability of capture by neon is greater, as expected from its capture cross sections reaching much higher energies. For a 50:50 mixture, the reduced ratios are similar, A(Ne,He) =3.36 for $\bar{p}$ and A(Ne,He) =3.69 for μ^-.

Upon closer inspection, there is a significant difference between the dependences on the mixture fractions in the two cases. The reduced capture ratio for $\bar{p}$ has a substantial monotonic dependence on the mixture, varying from 4.3 in predominantly helium to 2.7 in predominantly neon.

On the other hand, the reduced capture ratio for μ^-, shown in fig.7, is much less dependent on the mixture.

There have been a number of experimental determinations of capture ratios for helium and neon using μ^- and π^-. All of the capture ratios between ^4He and Ne have been determined indirectly, through measurement of ratios with some

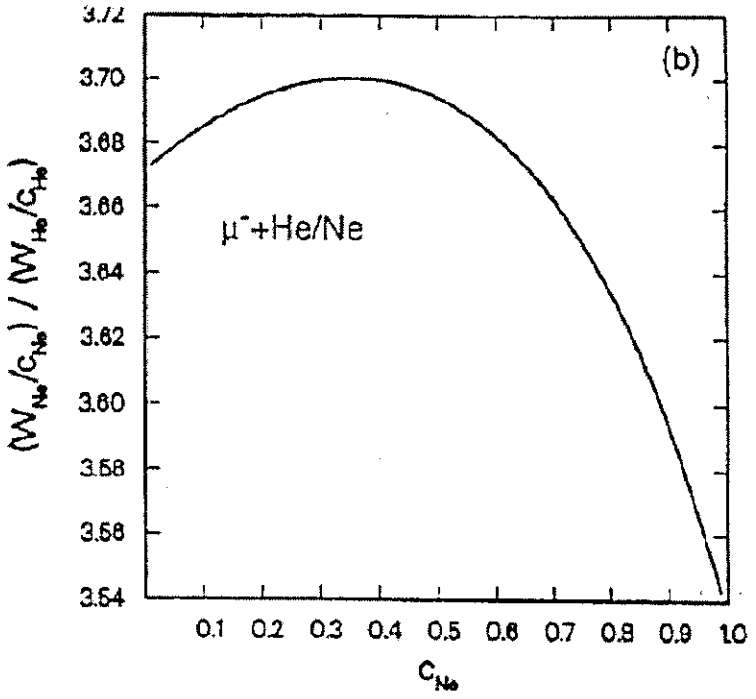

Figure 7: Reduced capture ratio for μ^- in He/Ne.

third species ($Ar, H_2, ^3He$).

The concentration dependence of the reduced capture ratios for neon and helium has not been measured experimentally. Measurements of the concentration dependence for μ^- capture in argon-neon, krypton-argon and xenon-argon mixtures have been reported [42]. For the first two mixtures, they found a significant concentration dependence, about as strong as for $\bar{p}$ in the neon-helium mixture. However, it is in the opposite direction; A(Ar,Ne) and A(Kr,Ar) increase as the fraction of the heavier element increases, while Cohen [41] finds A(Ne,He) decreases as the neon fraction increases.

Following Cohen, the oft-invoked quasiadiabatic arguments are still fairly descriptive of capture by helium, but are virtually useless for the ten-electron neon atom.

On the contrary, Schiwietz *et al* [43] described the stopping mechanism of negative particles in gas by the generalized adiabatic-ionization (AI) model. This model goes beyond the adiabatic model of Fermi and Teller [39, 40] by introducing collisional broadening into the electronic potential curves of the "quasidipole" that is transiently formed in low-velocity collisions of negative particles

c(Ne)	A(Ne,He)	$\overline{E}^{lab}_{capt}$(eV)		
		He	Ne	average
0.01	4.25	21.4	70.1	21.9
0.10	4.04	20.5	67.6	26.5
0.50	3.36	17.6	59.5	40.7
0.90	2.83	14.0	53.2	50.2
0.99	2.71	12.9	51.8	51.6

Table 1: Reduced capture ratios and average capture energies for $\bar{p}$ in neon-helium admixtures [41].

with atoms.
The AI model is seen to provide a good description of the He data in the whole velocity range below the stopping power maximum. When the nuclear stopping power $S_n^{\bar{p}}$ is added to the AI result for S_e, the total stopping power exhibits a minimum at that position where indications for a minimum are found in the data [44].
The ionization cross section for $\bar{p} + He$ collisions, and hence the electronic stopping power, exhibit a threshold at a velocity corresponding to a projectile energy of about 0.1 keV. In the total stopping power, this threshold is supposed to be masked under the nuclear stopping contribution. It appears however, that threshold effects may be discernible in the stopping in *heavy* rare gases. The electronic stopping power of low velocity negative particles is decisively influenced by the electron affinity of the "united atom:" formed in the collision (i.e., of the atom with nuclear charge number one unit less than that of the target atom).
As the nuclear stopping contribution is small in this v range, a steep rise of the stopping power in these targets is predicted to occur beyond v_{thr} (see Tab.2). Note that the position of the stopping power maximum is expected to depend only weakly on the target species. The threshold behaviour in heavy rare gas targets provides a signature of near-adiabatic electron dynamics in the stopping power of negative particles.

2 Strategy of the measurements

We intend to measure simultaneously annihilations on the same target nucleus at different momenta of the $\bar{p}$ taking advantage of the peculiar feature of the Streamer Chamber. Indeed, in this chamber the filling gas acts as detecting medium and also as reaction target. Moreover the filling gas works as degrader for the energy of the incoming $\bar{p}$, so increasing flight paths inside the chamber correspond to a lower average momentum of $\bar{p}$. For an average beam intensity of 20 $\bar{p}$ per bunch and per picture registered we expect to collect between 5 and

Target atom	⟨r⟩ (a.u.)	United atom	E_a (a.u.)	v_{thr} (a.u)
He^2(1s)	0.592	H^1	0.0276	0.065
Ne^{10}(2p)	0.664	F^9	0.1250	0.333
Ar^{18}(3p)	1.147	Cl^{17}	0.1331	0.609
Kr^{36}(4p)	1.392	Br^{35}	0.1235	0.688
Xe^{54}(5p)	1.700	I^{53}	0.1125	0.756

Table 2: Mean radius ⟨r⟩ of the target orbital initially occupied by the active electron, electron affinity E_a of the united atom and threshold velocity v_{thr} of the negative-particle stopping power in rare-gas targets [43].

10 events of annihilation in flight in ^4He for $\bar{p}$ momenta ranging between 100 and 30 MeV/c every $10^3\bar{p}$.
First of all, we intend to improve the accuracy of the measurement of the annihilation cross section in ^3He and in ^{20}Ne. The only measurements available on these nuclei at low energy are affected by a huge statistical uncertainty and need to be confirmed.
For this purpose we intend to operate the chamber at atmospheric pressure (or lower) with an admixture of noble gases of different atomic weight as $^{20}Ne-^3He$, $Xe-^4He$ and $Ar-^4He$. The percentages in the admixture will be a compromise between the opposite requirements of collecting quickly the desired number of annihilations on the heavier gas and of having a relatively long flight path of the $\bar{p}$. We intend to insert one or two thin CH_2 foils inside the streamer chamber at specific depths after the entrance window. Each target position will correspond to a specific average value of the $\bar{p}$ momentum at this depth. The annihilations which took place on C and H nuclei can be well identified and separated by checking the presence of nuclear fragments. In this way a direct measurement of the ratio between annihilation cross sections on the filling gas, on carbon and on the hydrogen can be performed by counting the observed annihilations. This method does not exhibit sources of relevant systematic errors since the measurements on the different nuclei are performed simultaneously by the same apparatus on the same solid angle and with the same beam set-up.
A direct comparison between the $\bar{p}$ annihilation cross section on hydrogen and the $\bar{p}$ elastic cross section on hydrogen can be done by identifying and measuring the $\bar{p}p$ elastic events in the CH_2 foils. The position of the foil inside the chamber fixes the average momentum of the impinging $\bar{p}$ and its width determines the corresponding momentum interval. A CH_2 foil will be used for the entrance window, allowing to collect annihilation and elastic scattering data in the interval 90-100 MeV/c, the first limit depending on the selected thickness of the entrance window.

The method followed for identifying and selecting the events is described below. Since the elastic scattering at small angles is dominated by Coulomb scattering (see fig.2,2), only events with medium and large scattering angle

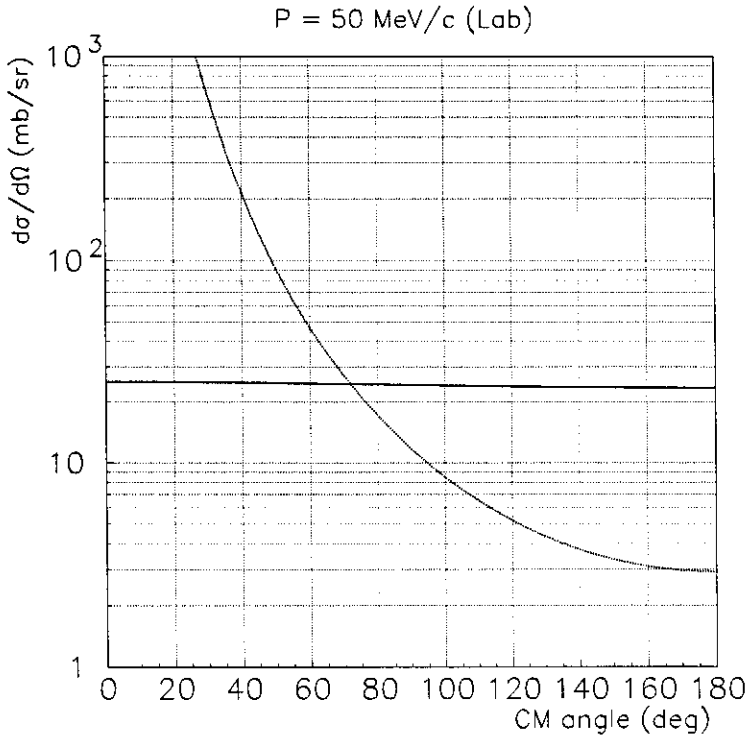

Figure 8: Angular distribution of the $\bar{p}p$ elastic cross section in C.M.S. at p_{lab} = 50 MeV/c . Full line: contribution of the strong interaction; dotted line: contribution of the Coulomb scattering.

can be attributed to the strong elastic channel. Among them, the very large angles are associated to a slow momentum of the recoiling antinucleon and to a correspondingly long range of the proton. In this case the event cannot be easily distinguished from an annihilation event on the C nucleus. With the cuts on scattering angles above described, in the momentum range $60 - 100$ MeV/c we estimate to be able to measure at least 50% of the $\bar{p}p$ elastic scattering events. According to available predictions [21] (see fig. 10), the $\bar{p}p$ elastic cross section in this momentum range amounts to 20% of the $\bar{p}p$ annihilation cross section, so we expect to collect 25 elastic scattering events on average on each foil every $3\ 10^5 \bar{p}$.
For the measurements of absolute cross sections the beam dose will be evaluated directly on each picture by counting the number of $\bar{p}$ tracks entering the selected

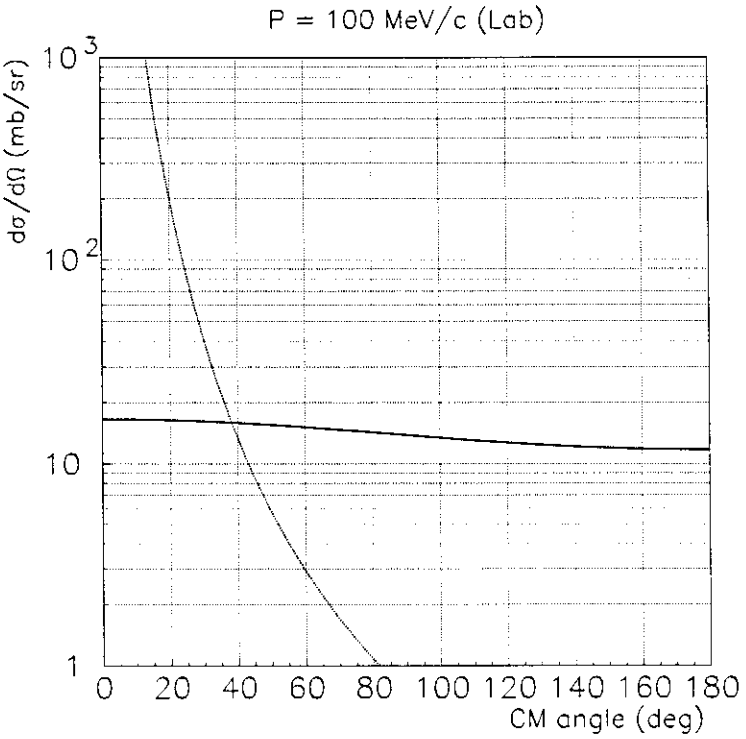

Figure 9: Angular distribution of the $\bar{p}p$ elastic cross section in C.M.S. at p_{lab} = 100 MeV/c. Full line: contribution of the strong interaction; dotted line: contribution of the Coulomb scattering.

fiducial volume.

2.1 Measurement of the $\bar{p}$ momentum

The streamer chamber in the proposed set-up is operated without magnetic field and the $\bar{p}$ momentum for annihilation events cannot be measured event by event. An average momentum at any depth can be attributed to a selected region of the target on the basis of the estimation of the $\bar{p}$ energy loss before the interaction vertex. During the last fifteen years, starting from the PS179 experiment we gained exclusive knowledge on the $\bar{p}$ stopping power in gases [44]. An independent complementary measurement of the $\bar{p}$ momentum can be done through the measurement of the elastic scattering events. Indeed in an elastic scattering event the momentum of the incoming $\bar{p}$ can be deduced from the

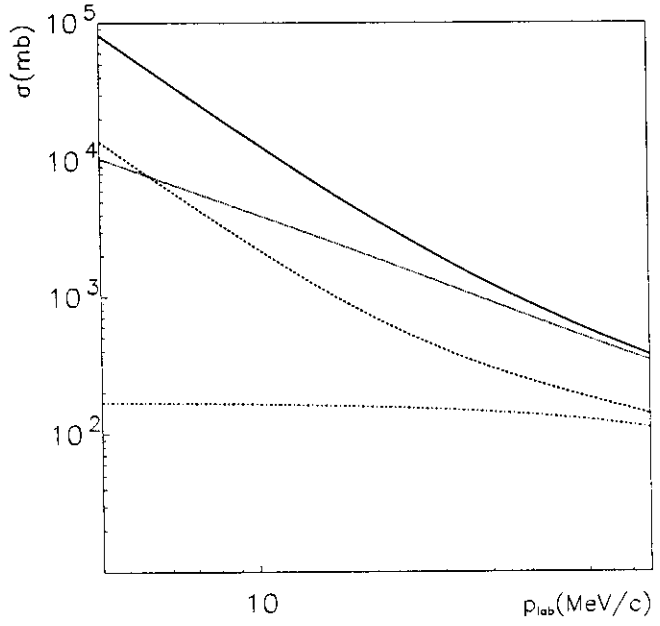

Figure 10: Continuous line: Total $\bar{p}p$ annihilation cross section calculated as in [21]. Dashed line: Total strong elastic cross section (the Coulomb forward singularity is excluded). Dotted and dot/dashed line: Total annihilation and elastic cross sections calculated after assuming zero charge for the projectile. At larger momenta the charge does not create large differences.

measurement of the relative angle formed by the two tracks outcoming from the vertex and from the measurement of at least one of the ranges of the outgoing particles. For this purpose only the events with two prongs identified will be selected. The $\bar{p}$ track will be tagged by the annihilation vertex at its end. Range measurement combined with ionization estimation will allow the identification of the recoiling nuclear fragment. $\bar{p}$ can scatter elastically on the nuclei of the filling gas and on C and H nuclei when the chamber is operated with the solid target inside.
Even if the scattering on any kind of nucleus can be used for the measurement of the scattering angle, the most accurate result is obtained for $\bar{p}$ scattered at medium-large angles on light nuclei, first of all on the proton. In these events the momentum transferred to the target nucleus may be as large as to imply for the corresponding recoil nucleus a path long enough to allow a careful measurement

of the recoil direction and range.

3 Experimental apparatus

The experimental apparatus to be installed in STRAD will include a self–shunted streamer chamber operated at a 1 atm pressure (or less [45]) of the filling gas (inert gases and small admixtures for regulating the size of the luminous centers along particle tracks) and a high-voltage pulse generator producing electric pulses of a few hundreds of kV required for operation of the streamer chamber. Such chambers developed by the INFN–JINR collaboration [46, 47, 48, 49, 50, 51] have been successfully used in studies of pion–helium (at JINR, Dubna) [52, 53] antiproton–helium and antiproton–neon interactions (LEAR, CERN exp. PS179) [54].

The STRAD streamer chamber will have an inner volume of 90 × 70 × 18 cm^3, so as to provide for particle registration within a solid angle amounting to $\sim 4\pi$.

The streamer chamber will be equipped with two CCD videocameras, recording antiproton-nucleus interaction events occurring in the chamber volume.

Actually, the streamer chamber serves simultaneously as a very thin target (the density of helium at NTP, for instance, is only 0.000178 g/cm^3) and as a tracking device, so it is a perfect vertex detector, since all slow secondary charged particles (in helium, protons of energies down to 0.5 MeV) produced in the reactions have quite visible and measurable tracks.

Ranges and energies for various charged particles in helium are reported in Table 3. Helium, like other inert gases, is a typical filling gas for the self-shunted streamer chamber.

Table 3: Energies (MeV) of various particles corresponding to given track ranges in ^{4}He at NTP

R (cm)	Particle:	π	p	d	t	^{3}He	α
1.0		0.16	0.17	0.17	0.14	0.25	0.3
5.0		0.27	0.55	0.70	0.75	1.70	1.8
10.0	(He)	0.40	0.85	1.20	1.30	2.90	3.3
	(Ne)	1.40	3.40	4.20	5.50	11.10	12.9
20.0		0.57	1.30	1.70	1.90	4.50	5.0

From Table 3 one can see that the range of a 1 MeV proton coming to a stop in helium exceeds 10 cm and is quite measurable; an α-particle with an energy of about 3.5 MeV has the same range.

The self-shunted streamer chamber technique permits obtaining well-localized ($\sim 2\,mm$ along the electric field) and highly luminous (by two orders of magnitude more than in conventional streamer chambers) charged particle tracks by addition to the filling gas of small amounts ($\leq 0.1\%$) of complex molecules (water vapour, hydrocarbons, etc.).

For operation of the streamer chamber electric pulses are applied that are few hundreds of kV; no special shaping of the high-voltage pulse applied to the electrodes of the chamber is required, and the shape of the pulse is determined by the electric discharge in the gas volume [46]. In our case, the positive pulse applied to the lower electrode of the chamber is $\sim$200 kV.

The high-voltage Marx pulse generator (HVPG) to be used is similar to the one applied in the CERN PS179 experiment [5] and will consist of 16 capacitor stages (made up of capacitors with $C = 0.05\ \mu$F) resulting in an output capacitance of $\sim$3100 pF. The delay of the output high-voltage pulse of the HVPG relative to the trigger pulse does not exceed $0.23\,\mu s$.

All videoregistration of nuclear events by experimental devices such as streamer chambers, permitting literal visualization of such events, has hitherto been performed with the aid of photographic techniques. These techniques involve mechanical apparatuses requiring maintenance, time-consuming development and actual measurement of the photographs of nuclear events for further image processing.

At present, highly sensitive sensors based on charge-coupled devices (CCD) are available on the market, which, together with the rapid development of computer technology, make possible immediate filmless registration of digitized images of nuclear events and further rapid data handling. The following characteristics of such images in the self-shunted streamer chamber have to be considered:

- their impulse nature requiring synchronization of the videosystem and the external pulse triggering the streamer system;
- the large dynamic luminosity range ($\leq$104) of the tracks;
- the high and irregular nature of background luminosity.

The system to be realized in STRAD will be similar to the one utilized by the DUBTO collaboration in a study of pion–helium interactions [8]: two high-resolution digital CCD videocameras will be used for obtaining stereo–images of nuclear events in the chamber. A possible choice is the SenSys–1400 videocamera from Photometrics Ltd.

The SenSys–1400 videocamera is based on a cooled CCD matrix with 1317×1035 photosensitive cells (pixels) of dimensions $6.8\times6.8\,\mu m^2$. The SenSys CCDs are

scientific-grade, exhibit good resolution, low noise, and linearity over the dynamic range and are used in scientific applications. The camera precision electronics, that converts the analog videosignal produced by the CCD into a digital signal, permits obtaining a 12-bit dynamic range (up to 4096 gray levels) for a noise level of $\sim 17e$ rms and a quantum efficiency of the photosensor amounting to $\sim$40%. The reset time is $\approx 1\ s$.

The entire system of registration, accumulation, and processing of images will comprise two digital SenSys videosensors connected to a Pentium processor, the software for processing and analysing images (Image–Pro Plus software for Windows), and storage devices for temporary and long-term recording of images on a 10 Gb HD and on 2 Gb removable hard disks Jaz.

The envisaged accumulation system will permit the registration and storage on removable disks Jaz of up to 1 per 2 second digitized image of pictures consisting of 1300×880 pixels, which will provide for the required resolution of 1 mm in the streamer chamber space.

Preliminary on–line data processing is also intended and includes scaling, storage, compression, and the creation of a database of images.

The database accumulated in the IPP system will be further applied for scanning and selection of useful events.

The above described system will be connected to Internet and open FTP access to the database for off–line data processing.

4 Experimental area

The experimental apparatus will be installed at the AD/CERN machine in the general purpose area (see fig.11) and will use the DEM beam line.

In this experimental area the apparatus will occupy in total an average square surface of $3 \times 4m^2$.
The apparatus will be completely shielded by a Faraday copper cage $3m$ high, properly grounded to avoid any electromagnetic noise to the surrounding instrumentation and to other experiments installed in the same hall. Concerning methods and performances of this solution we refer to our succesfull experience in the LEAR/CERN PS179 experiment.
In addition a control room $3 \times 4m^2$, possibly in the corner of the AD experimental hall, is needed. In this room we shall install the data acquisition system and we plan to monitor on line the performances of the apparatus.

The simple structure of the apparatus makes possible to install it on a movable support. The whole apparatus with related infrastructures can be mounted and dismounted in about one week.

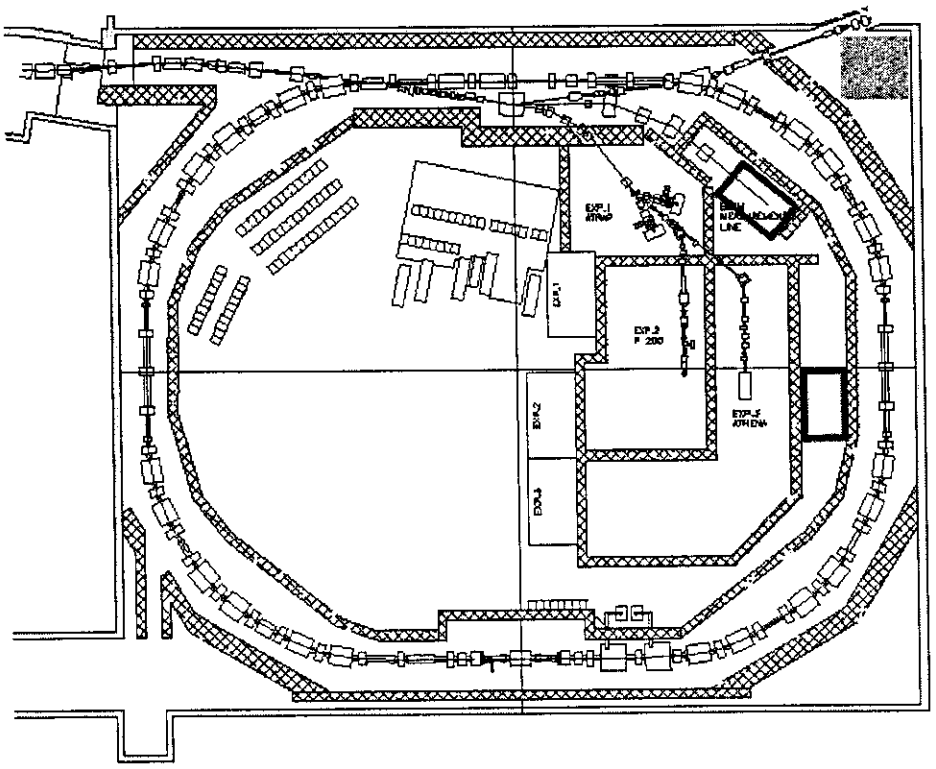

Figure 11: AD experimental area

5 Beam line and transport

The optimal matching between the AD bunched beam and our apparatus will be studied in agreement with the AD machine group. Anyway, a special wall with a collimator system will be studied to optimize the number and the trajectories of the $\bar{p}$ entering the Streamer Chamber.

6 Beam requirements

To perform the proposed measurements in the σ_{ann} sector with a statistical accuracy at 10% level about 350000 $\bar{p}$ in the Streamer Chamber are needed. Under the hypothesis of one bunch/min and of 20 $\bar{p}$/bunch in the Streamer Chamber, we need in total 300 hours of beam. It is equivalent to 30 nights (10 h/night) or 12 weekends (24 h/weekend).

The beam time may be in "self operating AD mode".
Moreover no more than half a day is needed to start the data taking without being in a stand-by and few minutes to be operative if in stand-by situation with respect to other experiments.
To take out the apparatus we need less than half a day.

7 Cost estimate[1]

	Description	KCHF
1	Streamer Chamber construction	8
2	Gas circulating system	17
3	Beam line and collimator	25
4	HV pulse generator	40
5	Faraday cage	16
6	TV cameras and DAQ system	64
7	Infrastructure	40
	Total	210

The ^3He gas needed for the experiment is already available in the Collaboration.

8 Experimental plans and milestones

2001
- apparatus construction. A prototype is not needed since well experienced technologies are adopted.
- project and construction of the beam line
- project and construction of the collimator wall

2002
- January-July
apparatus installation

- September-November
data taking on gaseous admixtures ($^3He/Ne$,$^4He/Ne$,$^4He/Ar$,$^4He/Xe$) and

[1] On September 22th the Istituto Nazionale di Fisica Nucleare has approved the cost planning of the experiment and has already allocated the whole budget required by the italian component of the Collaboration for the year 2001. The money will be released after the proposal approval by the CERN Committee

solid targets (CH_2)

end 2002 - beginning 2003
report on results obtained and discussion on a possible extension of data taking.

References

[1] CERN Courier, July/August 2000

[2] G.Bendiscioli and D.Kharzeev, Rivista del Nuovo Cimento **17** (1994) 1

[3] V.G.Ableev *et al.*, Il Nuovo Cimento **107 A** (1994) 943

[4] E.Botta, talk presented at LEAP2000 conference, Venice (2000)

[5] A.Zenoni *et al.*, Phys.Lett. **B 461** (1999) 413

[6] A.Zenoni *et al.*, Phys.Lett. **B 461** (1999) 405

[7] A.Bianconi *et al*, Phys.Lett. **B 481** (2000) 194

[8] A.Bianconi *et al*, in print on Phys. Lett. B

[9] M.Augsburger *et al*, Phys. Lett. **B 461** (1999) 317.

[10] S.Wycech et al., "Nuclear interactions of antiprotons: theory", in the proceedings of the conf. LEAP 98, Nucl. Phys. **A 655** (1999) 257c; Harmand et al., ibidem.

[11] R.Schmidt et al., Phys Rev C vol 60 , (1999) 0543309.

[12] S.Wycech, A.M.Green and J.A.Niskanen, Phys.Lett. **B 152** (1985), 308.

[13] G.Q.Liu, J.M.Richard and S.Wycech, Phys.Lett **B260** (1991) 15.

[14] Ye.S.Golubeva and L.A.Kondratyuk, Nucl.Phys. **B** (proc. suppl.) 56A (1997) 103.

[15] E.Friedman and A.Gal, Phys. Lett. **B 459** (1999) 43.

[16] E.Friedman and A.Gal, Nucl. Phys. **A 658** (1999) 345.

[17] K.V.Protasov, G.Bonomi, E.Lodi Rizzini and A.Zenoni, Eur.Phys.Jour. **A 7** (2000) 429.

[18] V.A.Karmanov, K.V.Protasov and A.Yu.Voronin, Nucl-th 0006041, submitted to Eur. Phys. J. **A**

[19] A.Bianconi, G.Bonomi, E.Lodi Rizzini, L.Venturelli and A.Zenoni, Nucl-th/9910031.

[20] A.Bianconi, G.Bonomi, E.Lodi Rizzini, L.Venturelli and A.Zenoni, Phys. Rev. **C 62** (2000) 014611

[21] A.Bianconi, G.Bonomi, M.P.Bussa, E.Lodi Rizzini, L.Venturelli and A.Zenoni, Phys. Lett. **B 483** (2000) 353

[22] A.Bianconi, G.Bonomi, M.P.Bussa, E.Lodi Rizzini, L.Venturelli and A.Zenoni, preprint Nucl-Th/0003006, submitted to EPJ.

[23] A.Bianconi, G.Bonomi, M.P.Bussa, G.Gomez, E.Lodi Rizzini, L.Venturelli and A.Zenoni, Nucl-th 0007053, submitted to Phys. Rev. **C**.

[24] A.Gal, E.Friedman and C.J.Batty, Nucl-th/0007029

[25] W.Brückner *et al*, Z.Phys. **A 339** (1991), 379.

[26] J.Haidembauer, T.Hippchen, K.Holinde and J.Speth, Z.Phys.**A 334** (1989), 467.

[27] A.S.Jensen, in "Antiproton-nucleon and antiproton-nucleus interactions", eds. F.Bradamante, J.-M.Richard and R.Klapish, Ettore Majorana international science series, Plenum Press 1990, p.205.

[28] S.Wycech, talk presented at LEAP2000 conference, Venice (2000)

[29] F.Iazzi et al., Phys. Lett. **B 475** (2000) 378.

[30] J.Carbonell, talk presented at LEAP2000 conference, Venice (2000)

[31] C.B.Dover, T.Gutsche, M.Maruyama and A.Faessler, Progr. Part. Nucl. Phys. **29** (1992) 87.

[32] C.Amsler and F.Myhrer, Ann. Rev. Nucl. Part. Sci. **41** (1991) 219.

[33] B.O.Kerbikov, L.A.Kondratyuk and M.G.Saposhnikov, Sov. Phys. Usp. **32** (1989) 739.

[34] T.Walcher, Ann. Rev. Nucl. Part. Sci. **38** (1988) 1.

[35] W.Weise, Nucl. Phys. **A558** (1993) 219c.

[36] A review on the Coupled channel model is given by I.S.Shapiro and a review on quark models by A.M.Green in "Antiproton-nucleon and antiproton-nucleus interactions", eds. F.Bradamante, J.-M.Richard and R.Klapish, Ettore Majorana international science series, Plenum Press 1990, pg.81 and pg.109.

[37] A.M.Green and J.A.Niskanen, International Review of Nuclear Physics, Vol.1, pg.570, World Scientific, 1984.

[38] J.J. De Swart and R. Timmermans, "The Antibaryon - Baryon interactions", Proceedings of the LEAP'94 Conference, World Sientific 1994, p.20.

[39] E.Fermi and E.Teller, Phys. Rev. **72** (1947) 399.

[40] A.S.Wightman, Phys. Rev. **77** (1950) 521.

[41] J.S.Cohen, Phys. Rev A**62**(2000)022512.

[42] P.Ehrhart et al., Phys. Rev. A**27**(1983)575; Z.Phys. A**311**(1983)259.

[43] G.Schiwietz et al., J. Phys. **B29**(1996)307; NIM **B115**(1996)106.

[44] A. Adamo et al.,Phys. Rev.A 47 (1993) 4517; M. Agnello et al.,Phys. Rev. Lett. 74 (1995) 371; OBELIX Collaboration, Phys. Rev. A 54 (1996) 5441–5444.

[45] " A Xenon Streamer Chamber and a Helium Chamber with Xenon Admixture", JINR Communication P13 - 8268, Dubna, 1974

[46] I.V.Falomkin et al.,Nucl. Instr. and Meth. **53** (1967) 266.

[47] F.Balestra et al., Nucl. Instr. and Meth. **125** (1975) 157.

[48] F.Balestra et al., Nucl. Instr. and Meth. **119** (1974) 347.

[49] F.Balestra et al., Nucl. Instr. and Meth. **131** (1975) 431.

[50] F.Balestra et al., Nucl. Instr. and Meth. **A234** (1985) 30.

[51] F.Balestra et al., Nucl. Instr. and Meth. **A257** (1987) 114.

[52] F.Balestra et al.,Nuovo Cim.**92** (1986) 139 and references quoted therein.

[53] E.M.Andreev et al., 16th International Conference on Few-body Problems in Physics, March 6–10, 2000, Taipei, Taiwan.

[54] Streamer Chamber Collaboration, "Study of the interaction of a low energy antiprotons with H,^2H,^3He,^4He,^{20}Ne and ^{40}Ar nuclei using a streamer chamber in a magnetic field" Proposal CERN/PSCC/80-123/P17 (1980).